Detecting Recompression of JPEG Images via Periodicity Analysis of Compression Artifacts for Tampering Detection

Yi-Lei Chen and Chiou-Ting Hsu, *Member, IEEE*

***Abstract*—Due to the popularity of JPEG as an image compression standard, the ability to detect tampering in JPEG images has become increasingly important. Tampering of compressed images often involves recompression and tends to erase traces of tampering found in uncompressed images. In this paper, we present a new technique to discover traces caused by recompression. We assume all source images are in JPEG format and propose to formulate the periodic characteristics of JPEG images both in spatial and transform domains. Using theoretical analysis, we design a robust detection approach which is able to detect either block-aligned or misaligned recompression. Experimental results demonstrate the validity and effectiveness of the proposed approach, and also show it outperforms existing methods.**

***Index Terms*—Compression artifacts, JPEG images, periodicity analysis, recompression detection.**

I. Introduction

With the wide availability of high-quality image editing software, general users can now easily edit or enhance digital image content in many ways. However, these easy-to-use image editing techniques also pose new challenges in digital forensics. Many passive or nonintrusive methods have been developed for detecting tampering in digital images. Some methods rely on detecting traces resulting from image acquisition or tampering operations, such as resampling [1], color filter array interpolation [2]–[4], camera sensor noise pattern [5], and scanner sensor noise [6]. Other methods attempt to analyze the inconsistencies in lighting direction [7] or statistical properties of natural images [8], [9]. Unfortunately, most existing methods are effective only for uncompressed raw images and are very vulnerable to JPEG compression. Since the JPEG image format has now been adopted in digital cameras and image processing software, it is vital to account for compression issues in tampering detection methods.

Manuscript received May 19, 2010; revised December 10, 2010; accepted January 03, 2011. Date of publication January 13, 2011; date of current version May 18, 2011. This work was supported by the National Science Council of R.O.C. under Contract NSC96-2628-E-007-142-MY3. The associate editor coordinating the review of this manuscript and approving it for publication was Dr. Adnan Alattar.

The authors are with the Multimedia Processing Laboratory, Department of Computer Science, National Tsing Hua University, Hsinchu, 30055, Taiwan (e-mail: fallcolor@gmail.com; cthsu@cs.nthu.edu.tw).

Color versions of one or more of the figures in this paper are available online at http://ieeexplore.ieee.org.

Digital Object Identifier 10.1109/TIFS.2011.2106121

Tampering in JPEG images often involves recompression and thus changes the original compression characteristics. Most existing tampering detection methods for JPEG images attempt to detect inconsistency in compression characteristics. Some rely on detecting inconsistency of JPEG quantization tables [10]–[13]. Others use the compression artifacts, either in spatial or frequency domain, as an inherent signature for JPEG images [14]–[18]. Although these approaches [10]–[18] adopt different compression characteristics, different methods have their restrictions and drawbacks. In the following subsection, we briefly summarize these approaches and their restrictions.

A. Inconsistency on Quantization Table

In a JPEG encoder, all 8×8 discrete cosine transform (DCT) blocks are quantized by the same quantization table before entropy encoding. Once a JPEG image is tampered with (for example, using the copy-move forgery), the tampered image may inherit the characteristics of quantization tables from different sources and thus may result in inconsistencies. In [10], the quantization table is estimated by quantization error minimization; in [11] and [12], the maximum likelihood estimation method [11] and the MAP approach [12] are proposed to estimate the JPEG quantization steps. Also, in [13], the authors pointed out that histogram of DCT coefficients concentrate only on multiples of quantization step and proposed to analyze the power spectrum of DCT coefficients for quantization table estimation. With the estimated quantization table, it is possible to detect block inconsistency and locate the tampered blocks. However, these methods tend to obtain a poor estimate of the primary quantization table (i.e., the quantization table of the original image) from the recompressed image once recompression is applied after tampering.

B. Abnormality of Compression Artifacts

When a tampered JPEG image is recompressed and again saved in JPEG format, the compression artifacts in the final image may differ from that of singly compressed images. These compression artifact abnormalities, either in spatial or frequency domain, have been used to detect recompression in JPEG images.

Luo *et al.* [14] proposed a spatial domain method to detect changes in the symmetric property of blocking artifacts for spatially shifted and recompressed images. Our earlier work [15] analyzed the blocking artifacts from their periodicity and proposed a blocking periodicity model to detect whether an

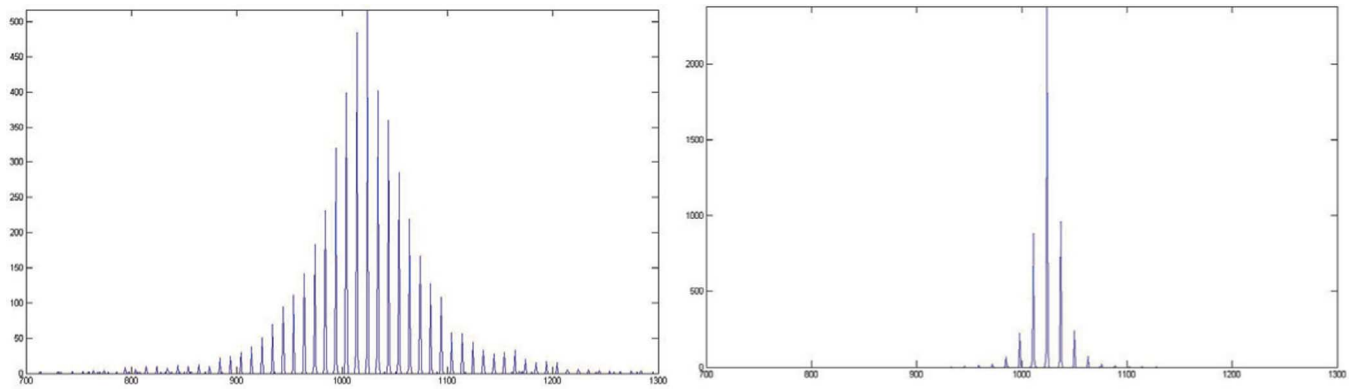

(a) (b)

Fig. 1. DCT coefficients histogram: (a) 2nd ac term with quantization step size $= 4$ and (b) 12th ac term with quantization step size $= 6$.

image has been cropped and recompressed. However, these spatial domain methods, which rely on detecting abnormality in blocking artifacts, are unable to detect recompression when there involves no spatially shift or cropping with misaligned block boundaries from the original JPEG image.

In frequency domain analysis, Benford's law has been used to model the statistical change in DCT coefficients caused by recompression [16], [17]. In [18], a method via DCT coefficient analysis is proposed to detect and locate doubly compressed regions. However, although these frequency domain methods try to detect abnormality in DCT distributions, they usually fail to detect recompression with misaligned block boundaries.

As is clear from the previous discussion (and to the best of our knowledge), no approach has been proposed for JPEG recompression detection that tackles both aligned and misaligned block boundaries. Considering that quantization table estimation completely relies on analysis of DCT coefficients, one would fail to measure the primary quantization table from recompressed images once there involves spatial shift with misaligned block boundaries. On the other hand, the spatial domain methods for detecting the abnormality of blocking artifacts would fail when the recompression includes no shifted or misaligned block boundaries. To the contrary, when the block boundaries in the recompressed images are misaligned from the original JPEG image, frequency domain methods usually fail to detect the abnormalities on DCT distributions.

In this paper, we assume the authentic images are originally in JPEG format and all tampering operations involve recompression. We propose a new compression characteristic that should be insensitive to either block aligned or misaligned cases, and then detect recompression in JPEG images using this proposed characteristic. In Section II, we describe the periodic characteristic of JPEG compressed images in mathematic formulation. In Section III, we further derive the variation of periodicity characteristics for doubly compressed JPEG images. Based on the periodicity characteristics discussed in Sections II and III, we then propose a robust recompression detection method in Section IV. A series of experimental results are presented in Section V to validate the effectiveness of the proposed method. Finally, we conclude in Section VI.

II. Periodicity Characteristics of JPEG Images

In the JPEG lossy compression standard, an input image is first divided into nonoverlapped 8×8 blocks, and each block is individually transformed using the DCT. The DCT coefficients are then quantized by a quantization matrix and finally encoded by the entropy coder. This block-based compression scheme inherently results in periodicity characteristics in both the spatial and DCT domains. In the spatial domain, since each block is individually transformed and quantized, the intensity inconsistencies between block boundaries may result in blocking artifacts. Especially in a heavily compressed image, blocking artifacts are comparatively noticeable every eight pixels and yield a regular periodic pattern in the spatial domain. In the DCT domain, since all blocks are quantized using the same 8×8 quantization matrix, coefficients of the same DCT term in the entire image are multiples of their corresponding quantization step. If we construct a histogram for each DCT term, then each of the 64 histograms would behave as a periodic signal. Note that the periodicity become less obvious with a large quantization step size, because most DCT coefficients will be quantized to zero. An example is shown in Fig. 1, where Fig. 1(a) and (b) are the histograms of the 2nd and the 12th ac terms (in zigzag scan order). From Fig. 1, histogram of lower frequency term shows a clear periodic pattern, while the periodicity in higher frequency term is less obvious.

Next, we will mathematically formulate the periodicity characteristics in spatial and DCT domains.

A. Periodicity of Blocking Artifacts

Blocking artifacts are caused by the intensity distortion between adjacent blocks after lossy compression. Let b denote the binary representation of the ideal blocking artifacts for an 8×8 block

$$b(i,j) = \begin{cases} 1, & \text{if } i \neq 8 \text{ and } j \neq 8 \\ 0, & \text{otherwise} \end{cases} \text{ where } 1 \leq i,j \leq 8 \quad (1)$$

where 1 indicates the area with consistent intensity and 0 indicates the blocking boundary. Hence, the binary representation

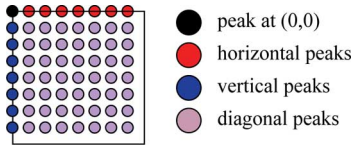

Fig. 2. The 8 × 8 peaks after discrete Fourier transform.

of blocking artifacts for a $M \times N$ JPEG image is represented as

$$B(x,y) = \left(1 - \sum_{m=1}^{M/T} \delta(x - mT)\right) \cdot \left(1 - \sum_{n=1}^{N/T} \delta(y - nT)\right) \quad 1 \le x \le M \quad 1 \le y \le N \tag{2}$$

where T indicates the periodicity of block coding, which equals eight in JPEG format.

In (2), we model the ideal blocking artifacts as a 2-D periodic pattern in spatial domain. Next, we analyze the spatial periodicity by conducting Fourier transform on $B(x,y)$ and obtain

$$\begin{aligned}\Gamma(u,v) &= \delta(u)\delta(v) \\ &\quad - \frac{1}{T}\left(e^{j2\pi v/N} \cdot \delta(u) \sum_{w=1}^{T} \delta\left(v - \frac{N}{T}w\right) + e^{j2\pi u/M} \cdot \delta(v) \sum_{h=1}^{T} \delta\left(u - \frac{M}{T}h\right)\right) \\ &\quad + \frac{1}{T^2} e^{j2\pi(ux/M + vy/N)} \cdot \sum_{h=1}^{T} \delta\left(u - \frac{M}{T}h\right) \cdot \sum_{w=1}^{T} \delta\left(v - \frac{N}{T}w\right).\end{aligned} \tag{3}$$

Equation (3) shows that $\Gamma(u,v)$ is nonzero only when u or v are multiples of M/T or N/T. Hence, there are $T \times T$ peaks in the Fourier domain of the ideal 2-D periodic signal $B(x,y)$ and the peak magnitudes are

$$|\Gamma| = \begin{cases} \left(1 - \frac{2}{T} + \frac{1}{T^2}\right), & (u,v) = (0,0) \\ \left(\frac{1}{T} + \frac{1}{T^2}\right), & (u,v) = \left(\frac{k_1 M}{T}, 0\right) \text{ or } \left(0, \frac{k_2 N}{T}\right) \\ \frac{1}{T^2}, & (u,v) = \left(\frac{k_1 M}{T}, \frac{k_2 N}{T}\right) \\ 0, & \text{otherwise} \end{cases} \tag{4}$$

where $1 \le k_1, k_2 \le T-1$. If we partition these 8 × 8 peaks into four regions, as shown in Fig. 2, then, from (4), the peak magnitudes are consistent within each region. Therefore, we conclude that the peak energy distributions characterize the periodicity of ideal blocking artifacts in the spatial domain and can be seen as an inherent signature of a singly compressed JPEG image.

B. Periodicity of DCT Coefficients

The distribution of block DCT coefficients on natural images has been shown to behave like Gaussian and Laplacian distributions for dc and ac coefficients, respectively. As shown in Fig. 3, although the quantized coefficients concentrate only on multiples of the quantization steps, the distribution remains the same even after the DCT coefficients are quantized. Therefore, we could formulate the distribution of quantized DCT coefficients in singly compressed JPEG images as

$$h_s(x) = q_1 \times L(x|0,\lambda) \times \sum_{n_1} \delta(x - n_1 q_1) \tag{5}$$

where q_1 indicates the quantization step size, $L(x|0,\lambda)$ denotes a zero-mean Laplacian distribution and λ is the Laplacian parameter. In (5), $h_s(x)$ is normalized by q_1 to ensure the probability integral equals to one.

We next analyze the periodicity in (5) by 1-D Fourier transform and obtain

$$\begin{aligned} H_s(\omega) &= \sum_{k_1=0}^{q_1} \frac{1}{1 + \left(\omega - \frac{2\pi}{q_1}k_1\right)^2 \lambda^2} \\ &= \begin{cases} 1 + \sum\limits_{\substack{0 \le k_1 \le q_1 \\ (k_1 \ne k)}} \frac{1}{1 + \left(\omega - \frac{2\pi}{q_1}k_1\right)^2 \lambda^2}, & \text{if } \omega = \frac{2\pi}{q_1}k. \\ \sum\limits_{k_1=0}^{q_1} \frac{1}{1 + \left(\omega - \frac{2\pi}{q_1}k_1\right)^2 \lambda^2}, & \text{else} \end{cases} \\ &= \begin{cases} 1 + \varepsilon_1(\omega), & \text{if } \omega = \frac{2\pi}{q_1}k \\ \varepsilon_2(\omega), & \text{else.} \end{cases} \end{aligned} \tag{6}$$

In (6), since $\varepsilon_1(\omega)$ and $\varepsilon_2(\omega)$ are near zero and negligible, the spectrum behaves like a periodic signal with constant peak magnitude on multiples of $2\pi/q_1$. An example is shown in Fig. 4. Thus, we could use the peak energy distribution to characterize the periodicity of DCT coefficients in the frequency domain.

Note that, although this periodicity exists in every quantized DCT coefficient, those DCT coefficients quantized by large quantization step sizes tend to concentrate only on a few peaks [as shown in Fig. 1(b)] and thus yield weaker periodicity in the Fourier domain [as shown in Fig. 4(b)].

III. Change of Periodicity Characteristics After Recompression

In Section II, we derived two periodicity characteristics for singly compressed JPEG images. In this section, we analyze how recompression may affect the above-mentioned characteristics. We assume all the source images are originally JPEG compressed and all the tampering operations will eventually involve recompression. Fig. 5 shows an example of copy-move tampering, where (x_1, y_1) and (x_2, y_2) are the upper-left coordinates of the region in the original and tampered images, respectively. As shown in Fig. 5, the copy-move tampering may result in misaligned block boundaries between the two JPEG images if $x_1 - x_2$ or $y_1 - y_2$ are not multiples of the block size. Otherwise, the tampered image would have aligned block boundaries. In addition, we assume that no matter what tampering operations are conducted on an image, the final step is to

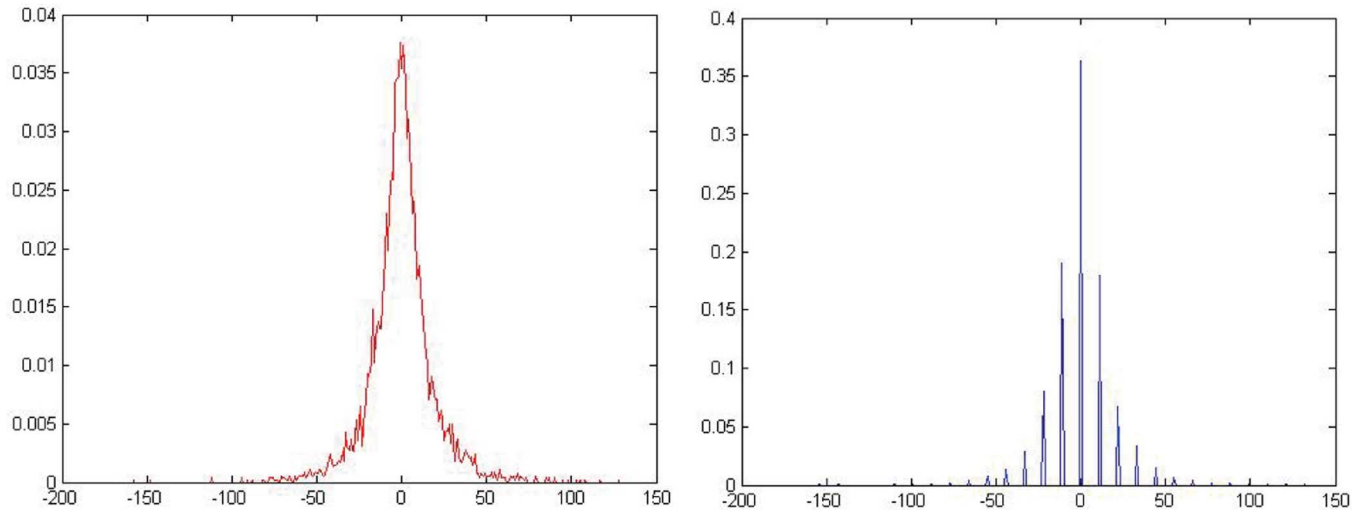

(a) (b)

Fig. 3. Distribution of first ac term: (a) unquantized DCT coefficients; (b) quantized DCT coefficients with quantization step $= 9$.

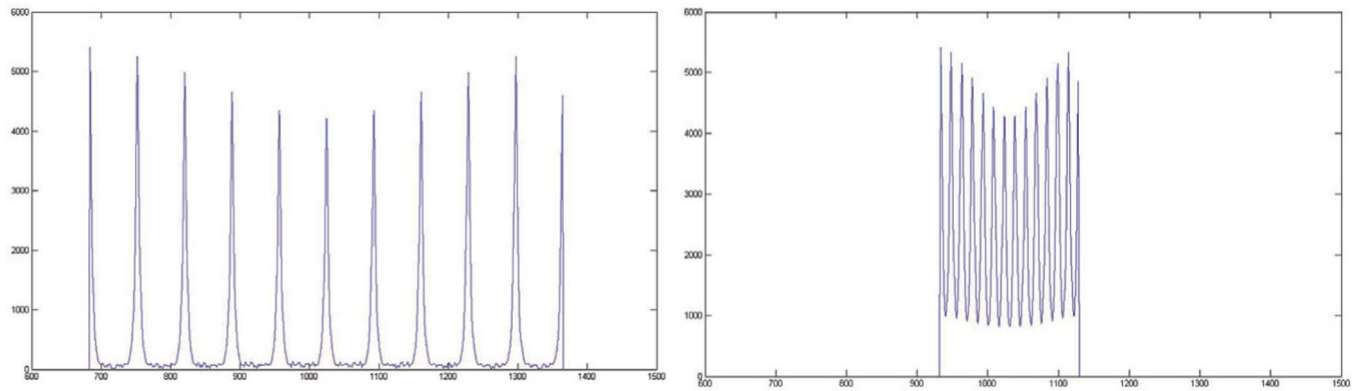

(a) (b)

Fig. 4. Fourier domain of Fig. 1(a) and (b), respectively.

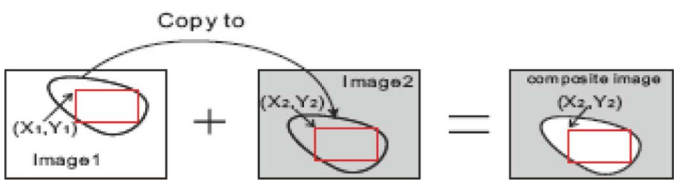

Fig. 5. Example of copy-move tampering [14].

save and recompress the tampered image as a new JPEG image. We will now discuss how recompression may change the two periodicity characteristics in the spatial and DCT domains.

A. Periodic Blocking Artifacts After Misaligned-Block Recompression

In a singly compressed image, blocking artifacts are located only on block boundaries, as indicated in (2). However, once an image has been tampered or cropped with misaligned block boundaries, the original blocking artifacts would shift along the cropping vector (dx, dy). Thus, we formulate the blocking artifacts in the cropped image (or subimage) as

$$B_C(x, y) = B(x - dx, y - dy) \tag{7}$$

where $dx \equiv x_1 - x_2 (\mathrm{mod} 8)$, $dy \equiv y_1 - y_2 (\mathrm{mod} 8)$; (x_1, y_1) and (x_2, y_2) are the coordinates in the original and spatially shifted JPEG images, respectively.

Note that, although blocking artifacts provide evidence of compression in the spatial domain, if $dx = 0$ and $dy = 0$ (i.e., aligned-block boundaries), we will not be able to detect any abnormalities in the blocking artifacts from the recompressed image. Therefore, here we only discuss the misaligned-block case, which means that after recompression, the original blocking artifacts would be located inside the blocks, but not along the block boundaries.

Fig. 6 shows the tampering operation with block-misaligned cropping and recompression. Since the strength of the original blocking artifacts would decrease after recompression, as shown

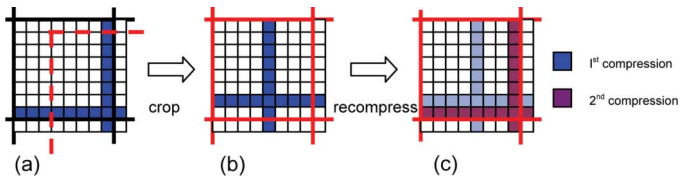

Fig. 6. Cropping and recompression operation: (a) the primary block with the first compression artifact; (b) after cropping, the blocking artifacts were shifted away from the block boundary; (c) after recompression, new blocking artifacts appear on the current block boundary, and the primary compression effect remains inside the block but with weaker strength.

in Fig. 6(c), we formulate the original blocking artifacts in the recompressed image as B_R

$$B_R(x,y) = \left(1 - \sum_{m=1}^{M/T} \alpha_m \delta(x - mT)\right) \cdot \left(1 - \sum_{n=1}^{N/T} \alpha_n \delta(y - nT)\right) \tag{8}$$

where $1 \le x \le M$, $1 \le y \le N$, and $0 \le \alpha_m, \alpha_n \le 1$. The parameters α_m and α_n indicate the decreasing degrees of the original blocking artifacts at the (m,n)th block. In order to obtain tractable results, we assume the decreasing degrees are block independent and rewrite (8) as

$$B_R(x,y) = \left(1 - \alpha \sum_{m=1}^{M/T} \delta(x - mT)\right) \cdot \left(1 - \alpha \sum_{n=1}^{N/T} \delta(y - nT)\right) \tag{9}$$

where $1 \le x \le M$ and $1 \le y \le N, 0 \le \alpha \le 1$. Now, with (2), (7), and (9), we assume the blocking artifacts in the first and second compressions are conditionally independent and then model the mathematical form of the two blocking artifacts in the recompressed image as B_{CR}

$$B_{CR}(x,y) = B_R(x - dx, y - dy) \cdot B(x,y). \tag{10}$$

Next, we again analyze the periodic characteristic by Fourier transform and derive the power spectrum of B_{CR}

$$|\Gamma_{CR}| = \begin{cases} \left|1 - \frac{Z_1+Z_2}{T} + \frac{Z_1 Z_2}{T^2}\right|, (u,v) = (0,0) \\ \left|-\frac{Z_1}{T} + \frac{Z_1 Z_2}{T^2}\right|, (u,v) = (0, \frac{k_2 N}{T}) \\ \left|-\frac{Z_1}{T} + \frac{Z_1 Z_2}{T^2}\right|, (u,v) = (\frac{k_1 M}{T}, 0), \\ \qquad 1 \le k_1, k_2 \le T-1 \\ \left|\frac{Z_1 Z_2}{T^2}\right|, (u,v) = (\frac{k_1 M}{T}, \frac{k_2 N}{T}) \\ 0, \qquad \text{otherwise} \end{cases} \tag{11}$$

where $Z_1 = 1\alpha^2 + 2\alpha\cos(2\pi u dx/M)$ and $Z_2 = 1\alpha^2 + 2\alpha\cos(2\pi v dx/N)$ if $dx \neq 0$ and $dy \neq 0$

From (11), we see that power spectrum is determined by the following factors: u, v, dx, and dy. Unlike (4), the peak magnitude will not always be consistent in the vertical, horizontal, and diagonal regions (as defined in Fig. 2).

B. Periodicity of DCT Coefficients After Aligned-Block Recompression

Assume a set of JPEG blocks is recompressed with misaligned block boundary. If we conduct DCT on these blocks, then the original periodicity caused by quantization will no longer exist. The reason is that these blocks now are composite of their original blocks and neighboring blocks. Since the newly calculated DCT coefficients are obtained from these composite blocks instead of the original JPEG blocks, we will not observe any of the original periodicity from analyzing the DCT histograms. On the other hand, if we analyze the DCT histograms on JPEG blocks recompressed with aligned block boundaries, then the original periodicity could still be observed. Therefore, here we only discuss the DCT periodicity for the case of aligned-block recompression.

Let q_1 and q_2 denote the quantization step sizes for the original JPEG compression and recompression, respectively; and c_0, c_1, and c_2 denote the unquantized DCT coefficient, the DCT coefficients after the original JPEG compression, and recompression, respectively. That is,

$$c_1 = q_1 \times \text{round}\left[\frac{c_0}{q_1}\right]$$

and

$$c_2 = q_2 \times \text{round}\left[\frac{c_1}{q_2}.\right]. \tag{12}$$

The quantization constraint set (QCS) theorem [19] showed that the DCT coefficients before and after compression would be bounded by

$$c_0 - \left\lfloor \frac{q_1}{2} \right\rfloor \le c_1 \le c_0 + \left\lfloor \frac{q_1}{2} \right\rfloor$$

and

$$c_1 - \left\lfloor \frac{q_2}{2} \right\rfloor \le c_2 \le c_1 + \left\lfloor \frac{q_2}{2} \right\rfloor. \tag{13}$$

From (12), the recompressed DCT coefficient c_2 is collected from the range $[-\lfloor q_2/2 \rfloor, \lfloor q_2/2 \rfloor]$ centered at c_1 and its distribution could be modeled as

$$h_d(x) = \sum_{n_2} \delta(x - n_2 q_2) \sum_{k=-\lfloor q_2/2 \rfloor}^{\lfloor q_2/2 \rfloor} h_s(x+k). \tag{14}$$

However, as there are rounding errors while conducting IDCT and DCT, we modify the distribution of the quantized DCT coefficient from $h_s(x)$ into $h'_s(x)$ by convolving the original formulation in (6) with a Gaussian distribution $N(x|0, 0.5^2)$. Finally, we substitute $h'_s(x)$ into (14) and obtain

$$h_d(x) = \sum_{n_2} \delta(x - n_2 q_2) \cdot \int_{k=[-q_2/2, q_2/2) \text{ or } (-q_2/2, -q_2/2]} h'_s(x+k) dk \tag{15}$$

where the range of k is determined by the sign of the coefficient x. We compare the simulation result from (15) with the

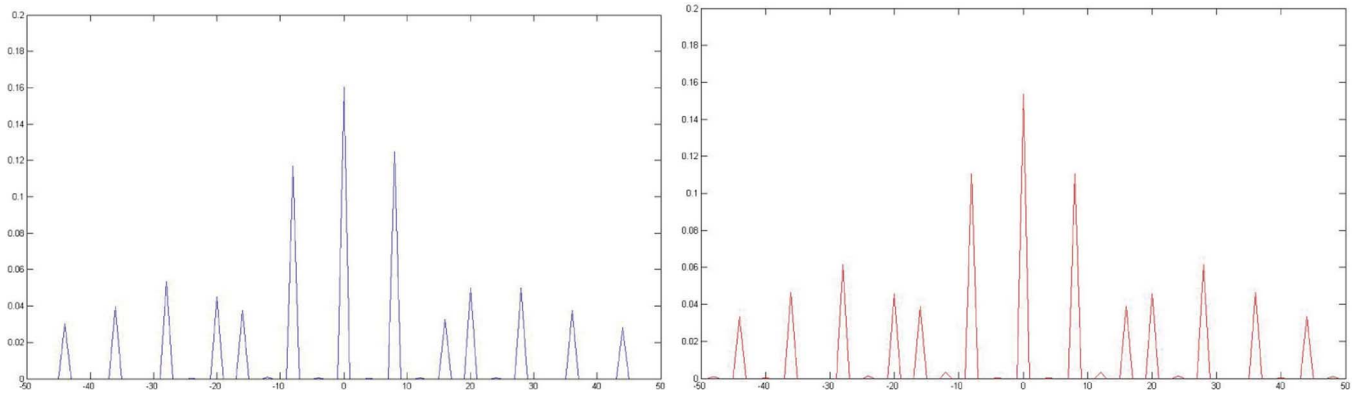

(a) (b)

Fig. 7. Distribution of doubly compressed DCT coefficients, where the first quantization step is equal to 9 and the second quantization step is equal to 4: (a) ground truth in JPEG image; and (b) the simulation result by (15).

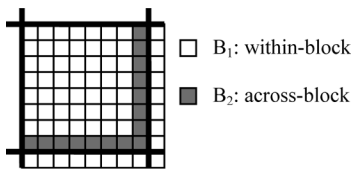

Fig. 8. Within-block pixels and across-block pixels in an 8 × 8 block.

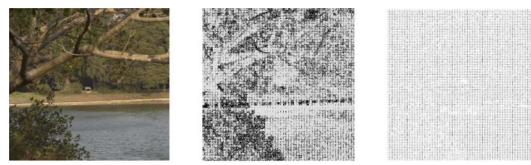

(a) (b) (c)

Fig. 9. (a) Original image; (b) probability map of (a) using the method in [15]; and (c) estimated blocking artifact of (a) with our proposed approach.

ground truth distribution of doubly compressed DCT coefficients in Fig. 7. The results in Fig. 7 show that our formulation indeed approximates the ground truth reasonably well.

Next, as in Section II-B, we analyze the periodic characteristics of $h_d(x)$ by Fourier transform. In order to simplify the calculation, here we ignore the rounding errors and obtain the frequency response $H_d(\omega)$ from (14)

$$H_d(\omega) = 2\pi \sum_{k_2=0}^{q_2} \sum_{k_1=0}^{q_1} \frac{1}{1 + (\omega - 2\pi(\frac{k_1}{q_1} + \frac{k_2}{q_2}))^2 \lambda^2} \times \frac{\sin\theta}{\theta}$$

where

$$\theta = \frac{q_2}{2}(\omega - \frac{2\pi}{q_2}k_2). \tag{16}$$

From (16), $H_d(\omega)$ has a higher magnitude (i.e., the observed peak) when ω is a multiple of $2\pi/q_1$ or $2\pi/q_2$. However, since $\sin\theta/\theta$ is close to one when θ is nearly zero, the magnitudes of $H_d(\omega)$ at multiples of $2\pi/q_2$ are much larger than at multiples of $2\pi/q_1$. That is, the peak magnitudes would not remain consistent once a JPEG image is doubly compressed.

IV. Detecting Recompression Via JPEG Periodic Characteristics

In Sections II and III, we have discussed the periodicity of blocking artifacts and DCT coefficients for singly and doubly compressed JPEG images. Next, in this section, we will present our proposed recompression detection method in terms of the periodicity in JPEG images.

When dealing with color images, we could conduct the detection on three color components independently. However, since the two chromatic components Cb and Cr are coarsely sampled and quantized in JPEG standard, their periodicity tends to be poorly characterized than in Y component. Therefore, we will conduct the detection method on Y component only.

A. Detecting Misaligned-Block Recompression by Blocking Artifacts

1) Estimation of Blocking Artifacts: Since our periodicity analysis of blocking artifacts rely on the binary representation of ideal blocking artifacts, we now describe how we estimate the blocking artifacts from JPEG images. We first use a simple method [11] to measure the local pixel difference $f(x, y)$ as

$$f(x, y) = I(x, y) + I(x+1, y+1) - I(x+1, y) - I(x, y+1) \tag{17}$$

where $I(x, y)$ is the intensity of the pixel (x, y). Next, if we classify pixels into two classes: within-block pixels and across-block pixels (as shown in Fig. 8), then the local pixel differences $f(x, y)$ of within-block pixels are usually highly similar to each other within a small neighborhood. Therefore, in our earlier work [15], we assume that there exists a local linear dependency of $f(x, y)$ for all within-block pixels. However, the assumption for linear dependency of blocking artifacts is oversimplified for complex images. Our simulation results show that the estimated blocking artifacts are highly content-dependent, as shown in Fig. 9(b), because the linear dependency model derived from the whole image may not apply to local characteristic of different pixels in complex images.

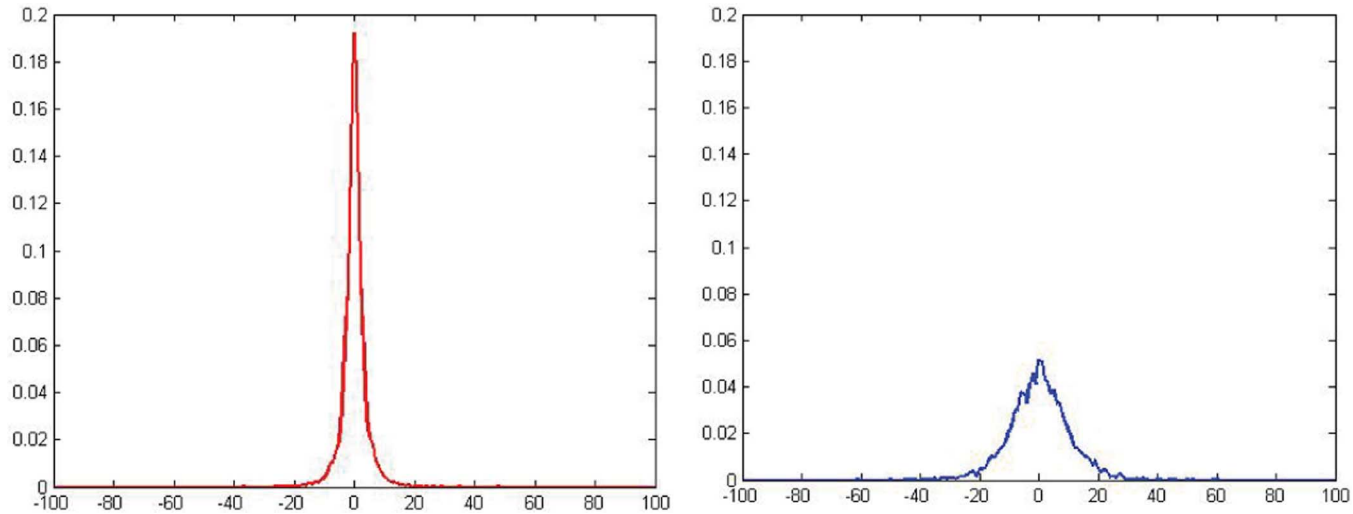

Fig. 10. Pixel difference distribution: (a) at block position (0,0); and (b) at block position (7,7).

Therefore, instead of using the linear dependency model, here we propose to model the blockiness in terms of both the local pixel difference $f(x,y)$ and its interblock correlation. Assume we decompose an image into nonoverlapped 8 $\times$ 8 blocks and construct 64 distributions $F_{i,j}(0 \leq i,j \leq 7)$ of pixel difference across the whole image. Although the 64 distributions may behave differently, depending on the image content, the distributions for the within-block pixels tend to concentrate around zero, as shown in Fig. 10(a). On the other hand, the distributions for across-block pixels usually have a larger variance, as shown in Fig. 10(b). Here, we represent these distributions by nonparametric histograms and define the pixel likelihood to the corresponding distribution by

$$p(f(x,y)|F_{k(x),k(y)}) = F_{k(x),k(y)}(f(x,y))$$

where

$$k(x) = x \bmod 8. \tag{18}$$

If we observe both the pixel difference $f(x,y)$ and its likelihood $p(f(x,y)|F_{k(x),k(y)})$, we find that pixels located on image edge or texture area usually have larger $f(x,y)$ but have smaller likelihood. Therefore, we can construct a better content-independent model to estimate blocking artifacts by including both $f(x,y)$ and its likelihood. We measure the distance between two adjacent pixels $f(x_1,y_1)$ and $f(x_2,y_2)$ as

$$\begin{aligned}&\mathrm{dist}(f(x_1,y_1),f(x_2,y_2))\\&\quad=|f(x_1,y_1)-f(x_2,y_2)|\\&\qquad\times\Big|p(f(x_1,y_1)|F_{k(x_1),k(y_1)})\\&\qquad\quad+p(f(x_2,y_2)|F_{k(x_2),k(y_2)})\\&\qquad\quad-p(f(x_2,y_2)|F_{k(x_1),k(y_1)})\\&\qquad\quad-p(f(x_1,y_1)|F_{k(x_2),k(y_2)})\Big|\end{aligned} \tag{19}$$

where $F_{k(x_1),k(y_1)}$ and $F_{k(x_2),k(y_2)}$ are interblock distributions of pixels $f(x_1,y_1)$ and $f(x_2,y_2)$, respectively. The first term in (19) measures the absolute value difference between the two local pixel differences $f(x_1,y_1)$ and $f(x_2,y_2)$. The second term in (19) includes $p(f(x_1,y_1)|F_{k(x_1),k(y_1)})$ and $p(f(x_2,y_2)|F_{k(x_2),k(y_2)})$, which measure the confidence of each pixel to the corresponding interblock distribution, and $p(f(x_1,y_1)|F_{k(x_2),k(y_2)})$ and $p(f(x_2,y_2)|F_{k(x_1),k(y_1)})$, which measure the between-class likelihood. If $f(x_1,y_1)$ and $f(x_2,y_2)$ are highly similar in terms of blockiness, then $dist\,(f(x_1,y_1),f(x_2,y_2))$ would be close to zero.

Using (19), next we estimate the blockiness $D(x,y)$ by weighted averaging the distance between a pixel and its eight neighbors

$$D(x,y)=\sum_{i=x-1}^{x+1}\sum_{j=y-1}^{y+1} w(i,j)\cdot\mathrm{dist}(f(i,j),f(x,y)) \tag{20}$$

where $w(i,j)$ is the normalized weight proportional to the probability likelihood of pixel $f(i,j)$

$$w(i,j)=\frac{p(f(i,j)|F_{f(i,j)})}{\sum_{u=x-1}^{x+1}\sum_{v=y-1}^{y+1}p(f(u,v)|F_{f(u,v)})}. \tag{21}$$

In order to be consistent with the binary representation defined in (1), we modify (20) as follows:

$$\begin{aligned}D'(x,y)=1-\min\Bigg(1,\ &\sum_{i=x-1}^{x+1}\sum_{j=y-1}^{y+1} w(i,j)\\&\cdot\mathrm{dist}(f(i,j),f(x,y))\Bigg).\end{aligned} \tag{22}$$

Thus, $D'(x,y)$ would be close to one if $f(x,y)$ is highly similar to its neighbors.

Fig. 9(c) shows the result obtained by (22). As we expect, since the local pixel difference $f(x,y)$ of an across-block pixel

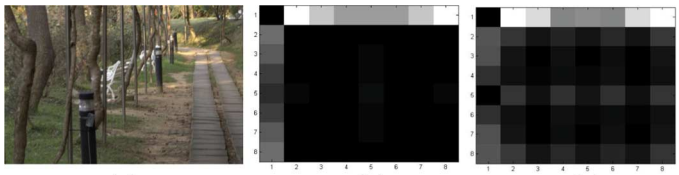

Fig. 11. (a) Original image; (b) peak window of (a), $QF = 80$; and (c) peak window of (a) with $QF1 = 60$ and $QF2 = 80$.

is usually dissimilar with its neighbors, its $D'(x, y)$ tends to be close to zero, which is indicated by a black pixel. Moreover, in comparison with the result of our earlier work in [15], the proposed estimate of blocking artifacts is more independent to image content and could better capture the inherent blockiness existing in JPEG images.

2) Feature Extraction in Fourier Domain: Next, we convert the blocking artifacts $D'(x, y)$ to Fourier domain. As shown in (3), we should observe 8 $\times$ 8 peaks in the power spectrum. In addition, from (4) and (10), a singly compressed JPEG image has consistent peak magnitudes within the horizontal, vertical, and diagonal regions (as defined in Fig. 2), while a recompressed image will not have consistent peak magnitudes. For example, in Fig. 11(b) and (c), we show the magnitudes of only the 8 $\times$ 8 peaks in the power spectrum for both the singly compressed and the recompressed image. Note that in Fig. 11, we ignore the strongest peak at the lowest frequency (0,0). As shown in Fig. 11(b), most peak magnitudes concentrate on vertical and horizontal regions and are evenly distributed within each region. On the other hand, in Fig. 11(c), since the blocking periodicity from the first compression also contributes to the estimate of blocking artifacts, the peak magnitudes now look very different from Fig. 11(b).

Therefore, we propose to extract features to measure the peak energy distribution so as to discriminate between singly compressed images and recompressed images. We calculate the normalized peak energy from three nonoverlapping regions R_v, R_h, and R_d, as defined in Fig. 2, and extract the following four features:

$$F_1 = \mathrm{std}\left(\frac{R_v}{\sum_{i=1}^{7} R_v(i)}\right)$$

$$F_2 = \mathrm{std}\left(\frac{R_h}{\sum_{j=1}^{7} R_h(j)}\right)$$

$$F_3 = \mathrm{std}\left(\frac{R_d}{\sum_{i=1}^{7}\sum_{j=1}^{7} R_d(i,j)}\right)$$

and

$$F_4 = \frac{\mathrm{mean}(R_d)}{\mathrm{mean}(R_v, R_h)}. \quad (23)$$

We will then use the four features to characterize the change of blocking artifacts caused by misaligned-block recompression.

B. Detecting Aligned-Block Recompression By DCT Periodicity

In Section II-B, we have shown that the histograms of DCT coefficients in a singly compressed JPEG image are periodic and the spectrum [as derived in (6)] are also periodic with constant peak magnitudes. On the other hand, as discussed in Section III-B, the histogram of DCT coefficients in the recompressed image has multiple periodicities and the spectrum no longer has constant peak magnitudes. Therefore, we first construct 64 histograms $h_{i,j}(0 \le i, j \le 7)$ for the 8 $\times$ 8 DCT coefficients individually and next derive the peaks from the corresponding spectrum $H_{i,j}$.

A simple peak extraction method is proposed here. For every power spectrum value $H_{i,j}(k)$, we use a search window w which involves $H_{i,j}(k-n)$ to $H_{i,j}(k+n)$, to detect whether $H_{i,j}(k)$ is a local maximum or not. Two empirical constraints are stated below

$$H_{i,j}(k) > \min(w) + \delta \quad \text{and} \quad H_{i,j}(k) > \frac{\max(H_{i,j})}{\alpha} \quad (24)$$

where n, α, and δ are parameters and are empirically set as $n = 1$, $\alpha = 5$, and $\delta = 0$.

Using the above constraints, we extract these local maxima as the peaks of $H_{i,j}$. Then we adopt standard deviation to show the periodicity variation; that is,

$$F_{i,j} = \mathrm{std}\left(\frac{P_{i,j}}{\max(P_{i,j})}\right) \quad (25)$$

where $P_{i,j}$ indicates all extracted peaks of $H_{i,j}$.

As we have demonstrated in Section II, when the DCT coefficients are concentrated on a few peaks in high frequency band, the periodicity becomes less easy to detect. Therefore, we only use the first five ac terms' DCT coefficients in zig-zag scan order to extract peak variation features.

Combining the four features in (23) and the five features in (25), we finally extract nine periodic features for JPEG recompression detection.

V. Experimental Results

To evaluate the proposed periodic features in JPEG images, here we focus on two tampering operations: 1) cropping and recompression, and 2) composite JPEG sources. All our experiments are conducted on the Y component of color images. In the first part, all the cropped image blocks reveal the primary compression traces of blocking artifacts in the spatial domain. Thus, we use the first experiment to validate the proposed four features in Section IV-A and compare to the related work [14] which also use spatial statistics. In the second part, local copy-move has been conducted; that is, the tampered images are composite of multiple JPEG sources. We use the nine periodic features in both the spatial and DCT domains to detect composite JPEG images. To show the superiority of our method, we also compare with two existing methods [17], [18], where [17] detects

TABLE I
DETECTION ACCURACY (%) OF SINGLE COMPRESSION (QUALITY FACTOR = $QF2$) AND DOUBLE COMPRESSION (1ST QUALITY FACTOR = $QF1$ AND SECOND QUALITY FACTOR = $QF2$)

QF1 \ QF2		70	75	80	85	90	95
50	Proposed	**80**	**85**	**92.5**	**97.5**	**100**	**100**
	BACM	78.5	83.5	90.5	93.5	95.5	95.0
60	Proposed	**76.25**	75	86.25	**97**	**100**	**100**
	BACM	73.5	79.5	86.5	92	94.75	95.0
70	Proposed	**72.5**	**76.25**	**81.25**	**95**	**100**	**100**
	BACM	68.75	73.5	78.75	89.75	95.0	95.5
80	Proposed	68.75	73.75	**82.5**	**92.5**	**100**	**100**
	BACM	72.25	73.75	79.5	91.75	94.5	95.5
90	Proposed	**70**	**71.25**	**81.25**	**95**	**100**	**100**
	BACM	65	70.25	76.5	86.75	94.5	95.75

doubly compressed images by Benford's Law, and [18] detects doctored JPEG images by double quantization effects.

Moreover, to validate the robustness of the proposed features under different distortions, we conduct a series of experiments for sensitivity analysis. We also evaluate the robustness of the proposed features using different sizes of pasted patch in copy-move tampering.

A. Detecting Cropping and Recompression

In this experiment, we use 250 color images captured using a Nikon D80 with RAW format and 3872 $\times$ 2592 resolution. We first compress these images with quality factor $QF2$, crop into size of 720 $\times$ 480 with aligned block boundaries, and use this data set as our singly compressed images. To create the cropped-and-recompressed images, we compress the RAW images with quality factor $QF1$, followed by randomly cropping into size of 720 $\times$ 480 and recompression with quality factor $QF2$.

Table I shows the detection accuracy with the proposed four features in Section IV-A and also a comparison with the BACM [14] method. The detection results in Table I show that our proposed method indeed outperforms BACM in most cases. Nevertheless, these features are feasible only when the original quality factor is smaller than the recompression quality factor. Otherwise, the former high quality compression information would be destroyed by recompression with lower quality factor. The cropping position also influences the detection accuracy. For example, if images are cropped along $(0, x)$ or $(x, 0)$ with $(0 \leq x \leq 7)$ before recompression, the previous blocking artifacts, which is especially large at position (7,7), would become less obvious to be detected. As shown in Fig. 12(b), if we crop images along $(0, x)$ or $(x, 0)$, most primary blocking artifacts will be merged into the second blocking artifacts, including the pixel difference at position (7,7). Therefore, the trace of original compression becomes less obvious compared with Fig. 12(a). After Fourier transform, the peak energy, instead of diverging to diagonal peaks, would still be distributed along vertical or horizontal peaks and retain consistency, making it an unreliable feature.

B. Detecting Composite JPEG Sources

In this experiment, we use 250 color images with RAW format, which were captured using Canon EOS, Nikon D80, and Pentax K100D. We first compress these images with quality factor $QF2$, crop into size of 1024 $\times$ 1024 with aligned block boundaries, and use this data set as our singly compressed images. To create the tampered image set, for each image S in the singly compressed image set with quality factor $QF1$, we randomly select another image with the same quality factor, crop a 720 $\times$ 720 patch, paste this patch to S, and then save the composite image as a new JPEG image T with quality factor $QF2$. Fig. 13 shows the copy-move operation. Note that all cropping positions are randomly selected and may result in either misaligned or aligned block boundaries. Thus, we have 500 images for each quality setting with $QF1$ and $QF2$. Using the nine features proposed in Section IV, we randomly select 400 images as training data to SVM, and use the rest as test data.

Table II shows the experimental results. We discuss the results in three cases, i.e., $QF1 < QF2$, $QF1 > QF2$ and $QF1 = QF2$. If $QF1 < QF2$, both blockiness and DCT features reveal the trace of recompression. If $QF1 > QF2$, blockiness features behave poorly since the pixel difference is

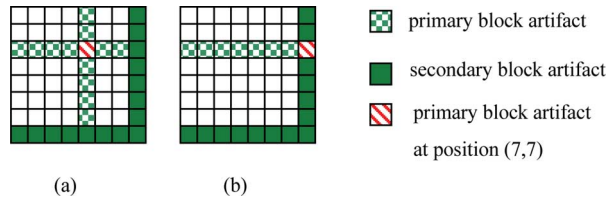

Fig. 12. Cropped and recompressed 8 $\times$ 8 JPEG block with different cropping vector. (a) cropping vector = $(5, 3)$ and (b) cropping vector = $(5, 0)$.

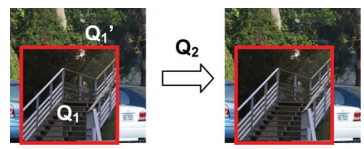

Fig. 13. Constructing a composite JPEG image, where the image size is 1024 $\times$ 1024, the size of the copy-move subimage is 720 $\times$ 720, and the cropping vector is randomly selected from (0,0) to (7,7).

TABLE II
DETECTION ACCURACY (%) OF COMPOSITE JPEG IMAGES

QF1 \ QF2		50	60	70	80	90
50	Proposed	**64**	**91**	**97**	**99**	**100**
	DQ effect	70	76	82	92	98
	Benford's Law	59	69	97	98	99
60	Proposed	**86**	**68**	**96**	99	**100**
	DQ effect	75	66	70	92	97
	Benford's Law	83	56	90	**100**	99
70	Proposed	75	**87**	**71**	**99**	**100**
	DQ effect	**77**	70	63	80	95
	Benford's Law	70	60	66	96	100
80	Proposed	**84**	**84**	**79**	66	**100**
	DQ effect	60	69	68	**74**	89
	Benford's Law	67	59	61	62	100
90	Proposed	71	**75**	**67**	**88**	77
	DQ effect	**73**	63	64	72	**78**
	Benford's Law	64	59	63	50	68

TABLE III
EXPERIMENTAL SETTING OF SENSITIVITY ANALYSIS

Level		1	2	3	4	5
White Gaussian noise		$\sigma = 0.5$	$\sigma = 1.0$	$\sigma = 1.5$	$\sigma = 2.0$	$\sigma = 2.5$
Blurring (Gaussian kernel)		$\sigma = 0.2$	$\sigma = 0.4$	$\sigma = 0.6$	$\sigma = 0.8$	$\sigma = 1.0$
Rotation (degree)		15°	30°	45°	60°	75°
Pasted patch	Size	180×180	360×360	540×540	720×720	900×900
	(%)	3	12	28	49	77

less discriminative as the quality factor decreases. Also, DCT features poorly characterize the periodicity variation since the periodicity is dominated by the second quantization step. Note that, whether $QF1 > QF2$ or $QF1 < QF2$, the proposed DCT features are both ineffective when

$$q_2 = mq_1 \quad \text{or} \quad q_1 = mq_2, \quad \text{where} \quad m \in N, q_1 \quad \text{and} \quad q_2 \quad \text{indicate the first and second quantization steps.} \tag{26}$$

In (26), when one quantization step is a multiple of the other, the histograms of the corresponding DCT coefficients would reveal only one single periodicity either from the first or second compression. Nevertheless, these cases in (26) rarely happen simultaneously for all the 64 DCT coefficients and thus we could still obtain sufficient features to discriminate periodicity change. The average detection rates of $QF1 > QF2$ and $QF1 < QF2$ are 98% and 80%, respectively. As we expect, our proposed features are robust to detect recompression.

Nevertheless, the average detection accuracy is merely 70% when $QF1 = QF2$. Since the first and second quantization step sizes are the same, it is impossible for DCT features to distinguish the primary periodicity. Only the blockiness features are valid when the primary blocking artifacts locate inside an 8×8 block, which implies that misalignment must always be present. With these constraints, we expect that the detection rate decreases much noticeably in this special case.

Furthermore, we compare our periodic features with the existing methods in [17] and [18]. Since the method in [17] applied the first digit distribution of DCT coefficients and requires a large amount of information for statistical analysis, this work is not reliable for detecting locally tampered images. Similarly, the method in [18] also relies on statistic features of double quantization effects, and thus requires a sufficient number of tampered blocks for reliable detection. Table II compares the detection accuracy with [17] and [18] using the fixed-sized pasted patch. As shown in Table II, our proposed features outperform [17] and [18] in $QF1 < QF2$, $QF1 > QF2$, and $QF1 = QF2$ cases.

C. Sensitivity Analysis

In this experiment, we use the composite JPEG images as our tampered data to validate the sensitivity of the proposed periodic features. The sensitivity analysis we conduct before recompression includes white Gaussian noises, blurring operation, rotation of the pasted patches, and copy-move tampering with different sizes of pasted patch. The experimental setting for this sensitivity analysis is listed in Table III, where the percentage (%) of pasted patch indicates the ratio of the copy-move patch in the whole image.

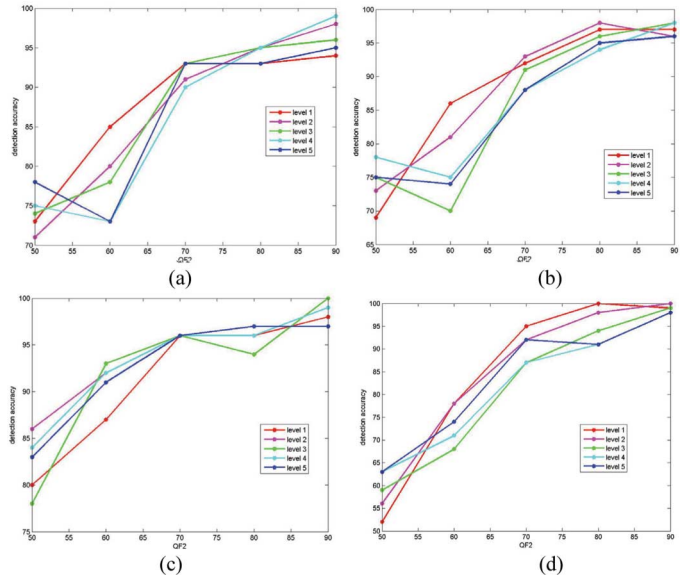

Fig. 14. Detection accuracy of composite JPEG images with (a) white Gaussian noise, (b) image blurring, (c) image rotation, and (d) different size of pasted regions.

Fig. 14(a)–(d) shows the detection accuracy with different levels of distortions or different sizes of pasted patch. We fix the quality factor $QF1$ of first compression as 50 to ensure $QF2$ is always larger than $QF1$. As shown in Fig. 14, our proposed periodic features are not sensitive to different distortion levels. Note that, when the size of pasted patch is smaller, more untampered blocks, which inherit recompression characteristics, are available. Therefore, as shown in Fig. 14(d), our proposed method works better with the smaller size of pasted patch. In addition, in Fig. 14(a) and (b), the detection rate does not always increase as $QF2$ increases when global operations such as additive white Gaussian noise or blurring are applied. Because global operation tends to change the intensities of all pixels and may destroy the primary compression artifacts, the remaining periodic features could be insufficient to characterize the recompression in either spatial or frequency domain. Therefore, our approach is limited if a global operation with a large distortion level is applied before recompression.

VI. CONCLUSION

In this paper, we considered tampering in JPEG images as a problem of detecting recompression. The main contributions of our work include: 1) we used mathematical formulation and theoretical proof to show that the periodicity of compression artifacts would change once a JPEG image is recompressed; 2) using this property, we further proposed a novel and robust approach for detecting recompression; and 3) combining the periodic features in both spatial and frequency domains, our method can detect recompression with either aligned or misaligned block boundaries. Experimental results show that the proposed method outperforms existing approaches in most quality factor settings.

REFERENCES

[1] A. C. Popescu and H. Farid, "Exposing digital forgeries by detecting traces of re-sampling," *IEEE Trans. Signal Process.*, vol. 53, no. 2, pt. 2, pp. 758–767, Feb. 2005.

[2] A. C. Popescu and H. Farid, "Exposing digital forgeries in color filter array interpolated images," *IEEE Trans. Signal Process.*, vol. 53, no. 10, pt. 2, pp. 3948–3959, Oct. 2005.

[3] A. Swaminathan, M. Wu, and K. J. R. Liu, "Non-intrusive component forensics of visual sensors using output images," *IEEE Trans. Inf. Forensics Security*, vol. 2, no. 1, pp. 91–106, Mar. 2007.

[4] H. Cao and A. C. Kot, "Accurate detection of demosaicing regularity from output images," in *Proc. IEEE Int. Symp. Circuits and Systems*, 2009, pp. 497–500.

[5] J. Lukas and J. Fridrich, "Digital camera identification from sensor pattern noise," *IEEE Trans. Inf. Forensics Security*, vol. 1, no. 2, pp. 205–214, Jun. 2006.

[6] H. Gou, A. Swaminathan, and M. Wu, "Intrinsic sensor noise for forensic analysis on scanners and scanned images," *IEEE Trans. Inf. Forensics Security*, vol. 4, no. 3, pp. 476–491, Sep. 2009.

[7] M. K. Johnson and H. Farid, "Exposing digital forgeries by detecting inconsistencies in lighting," in *Proc. ACM Multimedia and Security Workshop*, New York, 2005.

[8] S. Lyu and H. Farid, "How realistic is photorealistic?," *IEEE Trans. Signal Process.*, vol. 53, no. 2, pp. 845–850, Feb. 2005.

[9] P. Zhang and X. Kong, "Detecting image tampering using feature fusion," in *Proc. IEEE Conf. Availability, Reliability and Security*, Fukuoka, 2009, pp. 335–340.

[10] J. Fridrich, M. Goljan, and R. Du, "Steganalysis based on JPEG compatibility," in *Proc. SPIE Multimedia Systems and Applications IV*, Denver, CO, Aug. 2001, pp. 275–280.

[11] Z. Fan and R. L. de Queiroz, "Identification of bitmap compression history: JPEG detection and quantizer estimation," *IEEE Trans. Image Process.*, vol. 12, no. 2, pp. 230–235, Feb. 2003.

[12] R. Neelamani, R. D. Queiroz, Z. Fang, and R. G. Baraniuk, "JPEG compression history estimation for color images," *IEEE Trans. Image Process.*, vol. 15, no. 6, pp. 1365–1379, Jun. 2006.

[13] S. Ye, Q. Sun, and E. C. Chang, "Detecting digital image forgeries by measuring inconsistencies of blocking artifact," in *Proc. ICME*, Jul. 2007, pp. 12–15.

[14] W. Luo, Z. Qu, J. Huang, and G. Qiu, "A novel method for detecting cropped and recompressed image block," in *Proc. ICASSP*, Apr. 2007, vol. 2, pp. 217–220.

[15] Y. L. Chen and C. T. Hsu, "Image tampering detection by blocking periodicity analysis in JPEG compressed images," in *Proc. MMSP*, Cairns, 2008, pp. 803–808.

[16] D. Fu, Y. Q. Shi, and W. Su, "A generalized Benford's law for JPEG coefficients and its applications in image forensics," in *Proc. SPIE, Security, Steganography, and Watermarking of Multimedia Contents IX*, San Jose, CA, Jan. 2007.

[17] B. Li, Y. Q. Shi, and J. Huang, "Detecting doubly compressed JPEG images by mode based first digit features," in *Proc. MMSP*, Cairns, 2008, pp. 730–735.

[18] J. He, Z. Lin, L. Wang, and X. Tang, "Detecting doctored JPEG images via DCT coefficients analysis," in *Proc. Eur. Conf. Computer Vision*, Graz, Austria, 2006.

[19] A. Zakhor, "Iterative procedures for reduction of blocking effects in transform image coding," *IEEE Trans. Circuits Syst. Video Technol.*, vol. 2, no. 1, pp. 91–95, Mar. 1992.

Yi-Lei Chen was born in Taipei, Taiwan, in 1985. He received the B.S. degree in computer science in 2007 and the M.S. degree in computer science in 2009, both from the National Tsing Hua University, Hsinchu, Taiwan. He is currently working toward the Ph.D. degree at the Department of Computer Science, National Tsing Hua University, Hsinchu.

His research interests are digital image forensics, and image/video analysis and processing.

Chiou-Ting Hsu (M'98) received the B.S. degree in computer and information science from National Chiao Tung University, Hsinchu, Taiwan in 1991, and the Ph.D. degree in computer science and information engineering from National Taiwan University (NTU), Taipei, Taiwan, in 1997.

She was a postdoctoral researcher with the Communication and Multimedia Laboratory, NTU, from 1997 to 1998. From 1998 to 1999, she was with Philips Innovation Center Taipei, Philips Research, as a senior research engineer. She joined the Department of Computer Science, National Tsing Hua University, Hsinchu, Taiwan, as an Assistant Professor in 1999 and is currently an Associate Professor. Her research interests include multimedia signal processing, video analysis, and content-based retrieval.

Prof. Hsu received the Citation Classic Award from Thomson ISI in 2001 for her paper "Hidden digital watermarks in images." She is currently an Associate Editor of *Advances in Multimedia*.